Scilight

*Sustainable Energy & Process Engineering*
https://www.sciltp.com/journals/sepe



*Article*

# Evaluation of Structural Modification in Eggshell Derived CaO Catalysts Induced by Aluminium-Ferric Oxide Incorporation for Biodiesel Production under Non-Optimized Conditions

Ravi Yadav, Komal Priya, Shreyashee Naveria, Amisha Kushwaha and Abha Mishra *

Biomolecular Engineering Laboratory, School of Biochemical Engineering, Indian Institute of Technology, Banaras Hindu University, Varanasi 221005, Uttar Pradesh, India
* Correspondence: abham.bce@itbhu.ac.in

**How To Cite:** Yadav, R.; Priya, K.; Naveria, S.; et al. Evaluation of Structural Modification in Eggshell Derived CaO Catalysts Induced by Aluminium-Ferric Oxide Incorporation for Biodiesel Production under Non-Optimized Conditions. *Sustainable Energy & Process Engineering* **2026**, *1*(1), 2.

Received: 15 July 2026
Revised: 20 October 2026
Accepted: 28 October 2026
Published: 16 November 2026

**Abstract:** The sustainability of biodiesel production from multiple fry leftover domestic oil (MFO) derived feedstocks is hindered by cost of catalyst, reusability and stability. This study, eggshell derived CaO and wet impregnated $Al_2O_3$-CaO and $Fe_2O_3$-CaO catalyst were synthesised by calcination at high temperature. These heterogeneous catalysts were utilised for the production of biodiesel from multiple fried waste domestic cooking oil. Structural and surface characterization was done by ATR-FTIR, XRD, SEM-EDS and BET analysis. Fatty acid methyl ester (FAME) was separately synthesised for each catalyst under the same non-optimised conditions and the formation of FAME was also confirmed by gas chromatography. The XRD result shows the presence of well-defined peak of CaO as the major crystalline phase in all catalyst which confirms the structural stability of CaO during modification. However, when aluminium and iron oxides are wet impregnated, peak broadening, peak shift and minor peak variations occur. This suggests the dispersion of $Al_2O_3$ and $Fe_2O_3$ on surface of CaO and formation of interfacial bonds. Identical reaction conditions were followed for each catalyst with $Al_2O_3$-CaO exhibiting the best catalytic property. The FAME yield for each catalyst was $Al_2O_3$-CaO (94.16 ± 0.69%), $Fe_2O_3$-CaO (83.98 ± 0.89%) and unmodified CaO (79.46 ± 0.65%). The superior activity of $Al_2O_3$-CaO and $Fe_2O_3$-CaO is due to favourable surface stabilisation by preserving the structural integrity and accessibility of basic sites instead of surface area enhancement. Resultantly, catalytic efficiency of the CaO derived from eggshells can be improved through simple modification with metal oxides. This indicates the feasibility and cost-effective process for the biodiesel production by using burned oil after multiple frying, without using catalyst with homogeneous property.

**Keywords:** wet impregnation; homogeneous; heterogeneous catalyst; CaO; FAME

## 1. Introduction

The continued dependency on fossil-derived diesel even after technological advancement present a familiar set of problems that still persist. This includes volatile pricing and supply insecurity that is difficult to justify in long term. Biodiesel, particularly fatty acid (FA) methyl esters (FAME) are the transient substitute because it can be integrated into existing diesel infrastructure with minimal modifications. Multiple fried left over domestic oil (MFO) is a sustainable biodiesel feedstock because it avoids the food/fuel conflict associated with edible vegetable

**Copyright:** © 2026 by the authors. This is an open access article under the terms and conditions of the Creative Commons Attribution (CC BY) license (https://creativecommons.org/licenses/by/4.0/).
**Publisher's Note**: Scilight stays neutral with regard to jurisdictional claims in published maps and institutional affiliations.

oils [1]. Global MFO generation is expected to exceed 50 million tonnes annually, with countries like India contributing a higher share due to dense urban populations and expansion of food sector [2]. Several studies have noted that when properly processed, biodiesel produced from MFO can offer reduced life cycle of greenhouse gas emissions as compared to petroleum diesel [3].

A major problem with MFO includes non-uniform nature of feedstock. The composition of MFO depends on cooking practices and duration of use and oil type. All these factors affect free fatty acid (FFA) content and moisture content in MFO. High FFA containing oil requires acid pretreatment before transesterification [4]. This adds complexity as well as extra cost to the process. However, when FFA levels are low then single step transesterification becomes feasible. Even in these cases, the selection of catalyst remains a critical challenge, the broader goal is to reduce waste and environmental burden through entire production chain. Homogeneous alkali catalyst such as KOH and NaOH are widely used for the transesterification reaction because their high reaction rate and mild operating conditions. Major limitation of homogeneous alkali catalyst includes difficult separation and large volume of wastewater usage during downstream processing [5,6]. These drawbacks mark the interest in heterogeneous catalyst. It offers easier recovery, reusability, and reduced downstream processing. Despite extensive research, many heterogeneous catalysts still struggle to match the activity of homogeneous bases under mild operating conditions.

In this context, calcium rich waste materials, particularly chicken eggshells have emerged as a catalyst precursor [7]. Eggshells are mainly composed of $CaCO_3$, which can be converted to CaO through the process of calcination. Several studies have reported promising biodiesel yield using eggshell-derived CaO under mild reaction conditions [8,9]. The usage of eggshell based catalyst also aligns with circular economy principles. Unmodified CaO catalyst have limitations like leaching of active species, sensitivity to moisture and $CO_2$, and gradual deactivation over repeated cycles have been reported [10]. To address these issues, recent work has been explored in relation to surface modification or wet impregnation with metal oxides which may improve structural stability, dispersion of active sites, and resistance to deactivation [11,12].

Catalytic properties of $Al_2O_3$-CaO and $Fe_2O_3$-CaO based catalyst has been linked to modified acid base properties that may influence transesterification kinetics [13,14]. The performance of such a catalyst is reported to vary over a wide range depending on the methodology of preparation, temperature of calcination, and percentage of metal loading. Calcination of the catalysts at high temperatures may improve the crystallinity as well as the basicity of the catalysts. However, it may also result in a reduction in the surface area of the catalysts due to sintering [15]. This is a trade-off situation that is recognised but not extensively studied, particularly for catalysts prepared from biogenic waste materials.

In view of the aforementioned limitations that are present in the catalysts prepared by the aforementioned methods, the present study proposes to explore the application of wet impregnated $Al_2O_3$-CaO and $Fe_2O_3$-CaO modified eggshell catalysts for the production of biodiesel from waste cooking oil containing low FFA. The catalysts are prepared by the wet impregnation method followed by calcination at high temperature. The structural properties are investigated by FTIR, SEM-EDS, XRD, and BET. Biodiesel synthesis is carried out under single-step transesterification conditions and produced FAME was analysed through Gas chromatography. Rather than proposing a fundamentally new catalytic concept, this work aims to clarify how simple compositional modifications to a waste derived CaO catalyst influence catalytic behaviour under realistic reaction conditions. In doing so, it seeks to contribute the incremental but practical insight into the broader term effect to make biodiesel production both technically viable and genuinely sustainable.

Several low-cost heterogeneous catalysts have been investigated for biodiesel production, including red mud, alumina-, silica-, and calcium carbonate-based systems. Red mud is particularly attractive as an industrial waste-derived catalyst because it contains catalytically relevant Ca-, Fe-, Al-, and Si-containing phases; however, its composition and mineralogical characteristics can vary considerably with bauxite source, making the contribution of individual active phases and batch-to-batch reproducibility difficult to control [16]. Alumina and silica provide useful high-surface-area supports, but their effective application in transesterification generally requires incorporation of alkaline active species. In K-loaded alumina, catalytic activity depends strongly on active-phase loading and calcination, with excessive loading potentially covering accessible basic sites [16]. Similarly, impregnation of KI onto mesoporous silica substantially reduced the accessible surface characteristics because of pore coverage by the loaded phase. Calcium carbonate represents an abundant and inexpensive calcium source; however, direct $CaCO_3$-catalyzed transesterification has been reported to require relatively high temperatures to achieve high conversion, while conversion to CaO requires high-temperature calcination [16]. These limitations highlight the need for catalyst systems that combine the low cost and availability of waste-derived materials with controllable composition, sufficient basic catalytic functionality, accessible active sites, and improved operational stability. The principal contribution of this work is the experimentally supported demonstration that simple wet

impregnation with $Al_2O_3$ or $Fe_2O_3$ can tune the surface chemistry and operational stability of waste-derived CaO, with $Al_2O_3$ providing a particularly favourable balance between active-site accessibility, structural stability and catalytic performance under non-optimized conditions. Beyond catalytic activity and reusability, the end-of-life management of CaO-based catalysts is important for establishing their overall sustainability. Spent CaO catalysts can potentially be regenerated by washing and thermal reactivation to remove deposited species and restore active CaO sites, while catalysts that are no longer suitable for regeneration may be stabilized or repurposed as calcium-rich materials. Previous studies have demonstrated the reactivation of aged CaO catalysts by thermal treatment and the repeated use of eggshell-derived CaO for biodiesel production, supporting the potential for extending catalyst lifetime and reducing solid-waste generation [17,18].

Recent studies have demonstrated that modification of waste-eggshell-derived CaO with different oxides or supporting phases can improve catalytic performance and reusability, including Ag-modified CaO, Zn-modified eggshell catalysts, Fe-containing bifunctional systems, and $Al_2O_3$-supported eggshell-derived calcium catalysts [19]. However, differences in catalyst preparation and reaction conditions make it difficult to isolate the specific influence of the modifier on the structure–performance relationship. Therefore, $Al_2O_3$ and $Fe_2O_3$ were selected in the present study as chemically distinct oxide modifiers to systematically examine how their incorporation into the same eggshell-derived CaO matrix affects surface structure, accessibility of basic sites, stability and biodiesel production under identical reaction conditions. This comparative strategy enables evaluation of whether catalytic enhancement is primarily associated with changes in surface area or with modification of the surface chemical environment and active-site accessibility [20–22].

## 2. Materials and Protocols

All the materials used in this research work directly without purification. Aluminium chloride ($AlCl_3$), ferric chloride ($FeCl_3$), and potassium hydroxide (KOH) were purchased from Sigma Aldrich, Bangalore, India. Methanol (99%) analytical grade was purchased from local vendor for transesterification; distilled water was prepared in the lab; hen egg shells were collected from the local portray farm. Multiple fries left over domestic oil (MFO) was collected from local food vendors in the vicinity of the Indian Institute of Technology (BHU), Varanasi, India.

### *2.1. Oil Processing*

Before using MFO, the waste oil was separated through filtration to eliminate suspended food particles and kept in airtight containers at room temperature. After filtration to remove suspended food particles and other insoluble impurities, the multiple-frying waste cooking oil (MFO) was thermally dehydrated by heating at approximately 110 °C for 2 h under continuous stirring to remove residual moisture. The dehydrated oil was subsequently cooled to the reaction temperature before being used for transesterification. The acid number of MFO was 0.42 mg KOH $mL^{-1}$ was determined.

### *2.2. Catalyst Synthesis*

#### 2.2.1. Synthesis of Eggshell Powder and Preparation of CaO Catalyst

Selecting eggshells as the CaO precursor and wet impregnation as the modification method aligns with established strategies for creating low-cost, waste-derived heterogeneous base catalysts for biodiesel production [23,24]. Eggshells were collected and washed cleanly in tap water to remove adhering organic residue and then rinsed with distilled water. The cleaned shells were dried in a hot-air oven at 100 °C, 12 h to remove any residual moisture. To produce a fine powder, dried shells were crushed and ball-milled and sieved (100 μm) to get uniformed particles. It has been demonstrated that mechanically reducing the particle size prior to calcination enhances the uniformity of thermal decomposition in biogenic $CaCO_3$ and improves the reproducibility of CaO-based catalysts [25].

Obtained powder was kept in muffle furnace to calcinate at 900 °C, 2 h under ambient conditions. Temperature was chosen to ensure complete conversion of Calcium carbonate ($CaCO_3$) to calcium oxide (CaO), as temperatures below 900 °C may leave $CaCO_3$ residues that could impair catalyst performance [26,27]. The obtained white powder (CaO) was cooled at room temperature. Figure 1 illustrates the catalyst preparation process. The precursor loading was selected based on a previously reported wet-impregnation strategy for preparing $Al_2O_3$- and $Fe_2O_3$-modified shell-derived catalysts for biodiesel production [28]. $AlCl_3$ and $FeCl_3$ were selected as the respective Al- and Fe-containing precursors because of their suitability for the aqueous wet-impregnation route and their prior application in the preparation of shell-derived $Al_2O_3$- and $Fe_2O_3$-modified biodiesel catalysts [28].

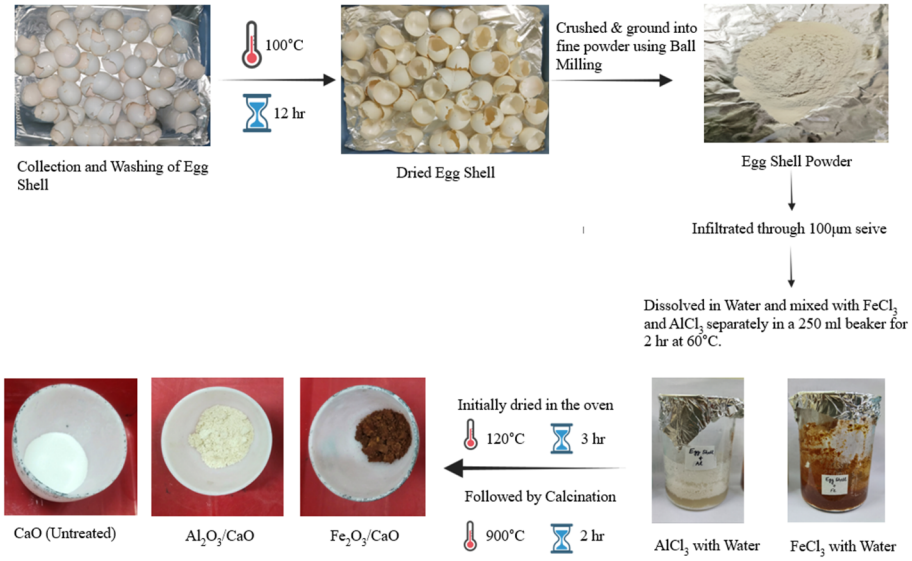


**Figure 1.** Catalyst preparation scheme: Diagrammatic representation of the synthesis route for eggshell-derived CaO, $Al_2O_3$-CaO, and $Fe_2O_3$-CaO catalysts, including washing, drying, calcination, wet impregnation, and high-temperature re-calcination steps.

### 2.2.2. Preparation of $Al_2O_3$-Eggshell Catalyst

$Al_2O_3$-CaO incorporated CaO eggshell catalyst was synthesised by adding 1.4 g of eggshell CaO powder by dissolving in 40 mL of distilled water by using electromagnetic dissolution. Subsequently, 0.6 g of aluminium chloride was gradually added to the solution. The addition of aluminium chloride induces effervescence, likely resulting from its reaction with carbonate groups in the eggshell powder. The mixture was stirred magnetically at 60 °C, 2 h to ensure proper catalyst impregnation. The mixture was subsequently dried in an oven at 120 °C for a duration of three hours. The catalyst was subsequently calcined at 900 °C for two hours in a muffle furnace. After calcination, the catalyst was allowed to cool naturally before being stored in a dry environment for future use [28,29].

### 2.2.3. Preparation of $Fe_2O_3$-Eggshell Catalyst

The $Fe_2O_3$-CaO modified eggshell catalyst was prepared using a procedure similar to that used for the $Fe_2O_3$-CaO modified eggshell catalyst. Briefly, 1.4 g of eggshell powder was dispersed in distilled water (40 mL) and slow addition of 0.6 g of ferric chloride ($FeCl_3$) under stirring. Effervescence was again observed, suggesting interaction between the iron salt and the carbonate rich eggshell matrix. The suspension was agitated at 60 °C for 2 h, dried at 120 °C, 3 h continued with calcination of 900 °C, 2 h; calcined and brought at normal temperature, stored under dry conditions pending further experimentation [28,30].

## *2.3. Production of Biodiesel (FAME)*

The biodiesel production process was continued through the transesterification of MFO by using the prepared eggshell based heterogeneous catalysts. Separate reactions were conducted for each catalyst system. All the experiments were continued with the employment of 4 wt%, catalyst loading that is relative to the MFO. MFO and methanol mixture was prepared in the molar combination of 1:8. MFO molecular weight was assumed ~874 g $mol^{-1}$ [31]. The catalyst and methanol were first mixed together and then introduced to the oil. The reaction was carried out in flask at 65 °C for 180 min with magnetic stirring at 300 rpm equipped with a reflux condenser [32]. The reaction was allowed to cool and settled, once it was completed. Enabled the separation of the biodiesel and glycerol layers. The biodiesel rich phase was collected carefully to minimize transfer of the glycerol phase and suspended catalyst. The separated biodiesel phase was then dried to remove residual methanol and moisture before analysis. The catalyst-containing fraction was processed separately according to the catalyst recovery procedure described in Section 2.5. FAME composition was determined by gas chromatography using the analytical procedure described in Section 2.4. The formula for the calculation of % yield for the biodiesel production is given below:

$$\text{Biodiesel Yield (\%)} = \frac{\text{Mass of biodiesel (gram)}}{\text{Mass of reactants (gram)}} \times 100$$

### *2.4. FAME Analysis by Gas Chromatography*

Gas chromatography analysis was done for the analysis of fatty acid methyl ester composition produced biodiesel. Gas chromatography (Centurion scientific, New Delhi, India) considering BPX70 capillary column. Argon gas was used as carrier having a ratio of 100:1. Initially the oven was heated at 140 °C for 5 min, then heated at a rate of 4 °C $min^{-1}$ until reaching 240 °C. The final temperature was held at 240 °C for 15 min to ensure the complete elution of FAME components [33].

### *2.5. Catalyst Reusability*

Synthesized catalyst was recovered in the bottom layer of the reaction system by using separating funnel. The material was then spun in a centrifuge at 5000 rpm for 10 min, followed by filtration. The catalyst was washed several times with methanol to remove leftover glycerol, unused oil, and any organic substances that had stuck to its surface. After washing, the catalyst was dried in a hot air oven at 100 °C for 4 h to get rid of any remaining liquid and moisture [18,34]. The dried catalyst was then used again in the next transesterification process under the same conditions without needing any extra chemical treatment. The catalyst reusability study was performed for five consecutive reaction cycles for each catalyst system.

### *2.6. Catalyst Characterization*

#### 2.6.1. ATR-FTIR Analysis

ATR-FTIR was performed using Agilent Cary 630 FTIR (Agilent technologies, Santa Clara, CA, USA). FTIR spectra were recorded in single-beam scan mode using 32 scans per sample. FTIR spectra were graphed in the range of 4000–650 $min^{-1}$ at a resolution of 4 $min^{-1}$ with a deuterated triglycine sulphate (DTGS) detector. Triangular apodization was applied, and phase correction was performed using the Mertz method [17].

#### 2.6.2. HR-SEM and EDS Analysis

Surface morphology and elemental composition of the synthesises hen egg sell based catalysts were inspected by using (SEM) scanning electron microscopy and powder X-ray dispersive spectrometry. HR-SEM was performed with a Nova Nano SEM 450 Instrument, manufactured by FEI Company of USA (S.E.A.) private limited and EDS analysis was proclaimed using Team Pegasus Integrated EDS-EBSD with Octane Plus and Hikari Pro (EDAX Inc., Mahwah, NJ, USA). Particle morphology and elemental distribution were evaluated by taking micrographs at 1000×, 1500× and 2500× magnifications [35].

#### 2.6.3. Powder X-ray Diffraction (HR-XRD)

High-resolution powder X-ray diffraction patterns were recorded to identify the different crystalline structures of the catalysts. HR-XRD was carried out using Rigaku Smart Lab 9 kW powder type (RIGAKU Corporation, Tokyo, Japan). The measurements were taken in the 2θ range of 10–70° with a step size of 0.02° and a scan rate of 0.5° $min^{-1}$ [36].

#### 2.6.4. BET Surface Area Analysis

BET analysis was used to find out the surface area, pore volume, and micropore volume of the catalysts. BET was performed using BELLSORP MAX II & BELCAT-II (MicrotracBEL Corporation, Osaka, Japan). Sample was heated at the target temperature of 400 °C and degassed for a soak time of 10 h. BET was performed for $N_2$ gas at absorption temperature of 77 K. Surface area was considered indicative of the availability of active sites, while pore volume provided insight into the accessibility of catalytic regions. Micropores, defined as pores smaller than 2 nm, were evaluated due to their relevance in reactions involving small molecular species [37].

## 3. Results and Discussion

### *3.1. FTIR Analysis*

FTIR spectra of CaO, $Al_2O_3$-CaO and $Fe_2O_3$-CaO catalysts as shown in Figure 2, reveal broadly similar profiles, indicating that the CaO framework derived from eggshells remains intact after metal oxide impregnation. The broad absorption observed in the 3600–3200 $cm^{-1}$ region across $Al_2O_3$-CaO and $Fe_2O_3$-CaO samples can be attributed to surface –OH groups and adsorbed moisture, which is difficult to eliminate completely for CaO-based materials exposed to ambient conditions [17]. The bands in the 1400–1500 and 850–880 $cm^{-1}$ regions are attributed to surface carbonate species formed through partial carbonation of CaO. In $Al_2O_3$-CaO, changes in the intensity/profile of the –OH and carbonate bands indicate modification of the surface chemical environment following $Al_2O_3$ incorporation. The low-wavenumber region shows metal–oxygen vibrations associated with Ca–O and Al–O species, although overlapping bands prevent definitive assignment of Ca–O–Al linkages from FTIR alone. These observations, together with XRD and SEM–EDS results, support successful $Al_2O_3$ incorporation into the CaO catalyst [20].

Weak bands in the 1450–1410 $cm^{-1}$ region are observed more dominantly in $Fe_2O_3$-CaO catalysts, suggesting the presence of residual carbonate species or partial re-carbonation of CaO. This behaviour is commonly reported for biogenic CaO and is consistent with surface interaction with atmospheric $CO_2$. Upon $Al_2O_3$-CaO and $Fe_2O_3$-CaO modification, additional features appear in the lower wavenumber region (~900–700 $cm^{-1}$), which may be associated with metal oxygen vibrations. These changes suggest surface modification rather than bulk structural transformation, an interpretation supported by XRD results [23,27].

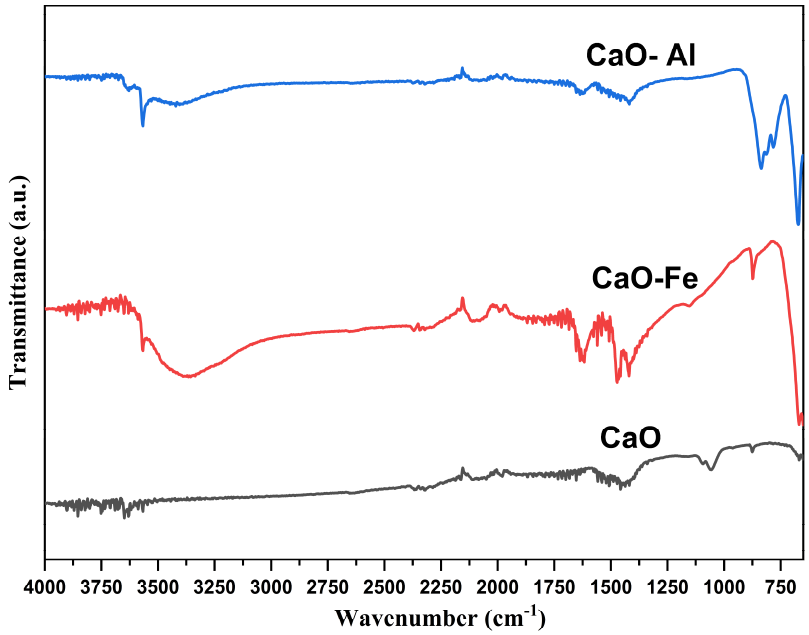


**Figure 2.** FTIR spectra: ATR FTIR spectra of CaO, $Fe_2O_3$-CaO, and $Al_2O_3$-CaO catalysts showing characteristic bands associated with surface hydroxyl groups, residual carbonate species, and metal oxygen vibrations, indicating preservation of the CaO framework after metal oxide modification.

### *3.2. XRD Analysis*

The XRD pattern for CaO catalyst (Figure 3a) shows that the peaks for the CaO catalyst are present at 2θ = 32.2°, 37.4°, 53.9°, 64.2°, and 67.4°. The peaks for CaO indicate that CaO crystallizes during high-temperature calcination. The additional peaks for $CaCO_3$ indicate that $CaCO_3$ is present. This is because $CaCO_3$ has additional peaks in the XRD pattern. The peaks for $CaCO_3$ indicate that $CaCO_3$ is present in the catalyst [17,23,27,38]. The XRD pattern for the $Al_2O_3$-CaO catalyst (Figure 3b) shows that the intensity of the characteristic peaks for CaO has decreased. The absence of characteristic peaks for $Al_2O_3$ indicates that $Al_2O_3$ is in an amorphous form. No characteristic peaks of $Al_2O_3$ can be observed, which indicates that $Al_2O_3$ exists on the surface of catalyst and does not affect the crystallinity of CaO. The XRD pattern for the $Fe_2O_3$-CaO catalyst (Figure 3c) indicates that additional characteristic peaks for $Fe_2O_3$ are present. The reduced intensity for the characteristic peaks for CaO indicates that $Fe_2O_3$ strongly interacts with CaO. The reduced intensity for the characteristic peaks for CaO indicates that $Fe_2O_3$ affects the surface of CaO [30]. The XRD patterns revealed distinct structural changes

following modification of CaO with $Al_2O_3$ and $Fe_2O_3$. The unmodified CaO catalyst was predominantly indexed to lime (CaO), confirming CaO as the major crystalline phase. In contrast, the $Al_2O_3$-modified CaO exhibited a strong match with mayenite ($Ca_{12}Al_{14}O_{33}$), indicating the formation of calcium–aluminate phases during calcination. The formation of mayenite from $Al_2O_3$-CaO systems during thermal treatment has been widely reported and is associated with solid-state reactions between CaO and $Al_2O_3$ [39]. For the $Fe_2O_3$-modified catalyst, the XRD pattern showed the strongest match with a Ca–Fe–O phase, together with additional reflections corresponding to related calcium–iron oxide/brownmillerite type phases. Calcium ferrite/brownmillerite phases such as $Ca_2Fe_2O_5$ are known to form through solid-state reactions involving calcium- and iron-containing precursors during thermal treatment [40]. These results suggest that $Al_2O_3$ and $Fe_2O_3$ interact with CaO during calcination, promoting the formation of mixed calcium–aluminate and calcium–iron oxide phases, respectively. Major diffraction peaks corresponding to CaO and secondary oxide phases has been shown in Table 1.

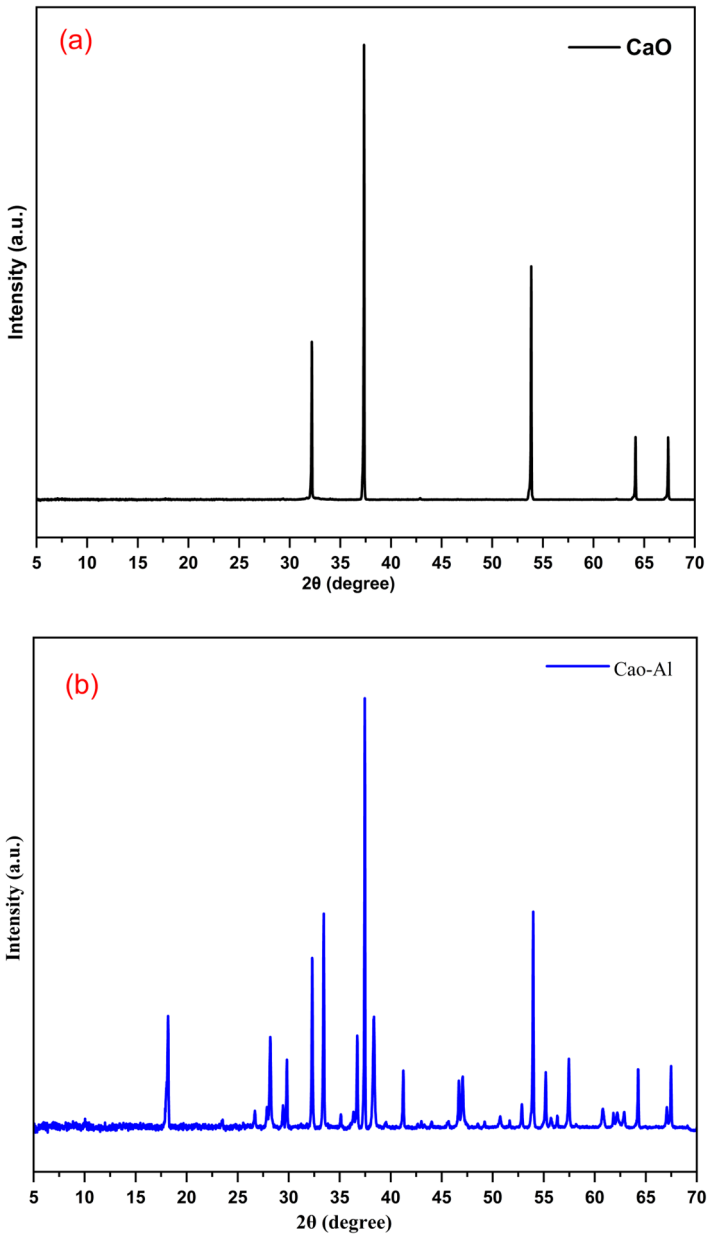


**Figure 3.** *Cont.*

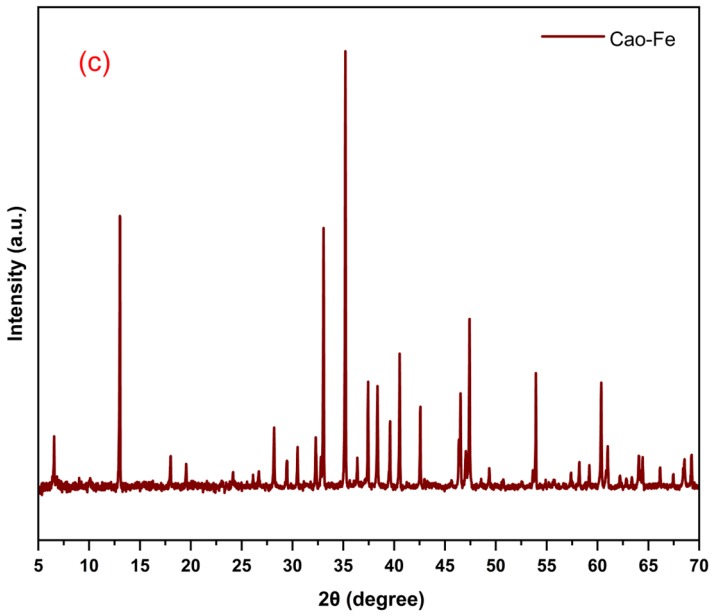


**Figure 3.** XRD analysis: (**a**–**c**) X-ray diffraction patterns of CaO, $Al_2O_3$-CaO, and $Fe_2O_3$-CaO catalysts, respectively, showing dominant CaO reflections and structural modifications induced by Al and Fe wet impregnation.

**Table 1.** Tabulated assignment of major diffraction peaks corresponding to CaO and secondary oxide phases.

| 2θ (Degree) | Peak Assignment | Importance |
|---|---|---|
| ~32.2 | (111) CaO cubic | Most intense; confirms pure CaO phase |
| ~37.3 | (200) CaO cubic | Highly crystalline, phase purity indication |
| ~53.8 | (220) CaO cubic | Confirms bulk cubic structure |
| ~64.1 | (311) CaO cubic | Marks high crystallinity, absence of major impurities |
| ~67.3 | Minor CaO reflections | Further confirmation of phase, possible minor secondary |
| ~47.2 | γ-$Al_2O_3$ or Al-rich phase | New/minor peaks, possible formation of alumina trace phases |
| ~43.5 | Fe oxide possible | Can indicate $Fe_2O_3$ or $Fe_3O_4$ phase |

### *3.3. SEM-EDS Analysis*

The surface morphology of the obtained catalyst was studied using Scanning Electron Microscopy-Energy Dispersive Spectroscopy (SEM-EDS). Figures 4–6 show the SEM micrograph and EDS spectra for CaO, $Al_2O_3$-CaO, and $Fe_2O_3$-CaO catalysts, respectively.

The SEM micrograph for CaO catalysts in their raw form, as shown in Figure 4a,b, and at higher magnification of 1000× and 1500×, shows that the catalysts are of irregular shape, have a rough surface, and are broken into pieces. The catalysts are also seen to be in a state of aggregation in a compact form, which shows that they do not have a pore structure. This is not unexpected for CaO catalysts, as they were prepared by calcining biogenic $CaCO_3$ at high temperature, resulting in the formation of CaO through a thermal decomposition process that does not produce a porous catalyst. The surface morphology of eggshell-derived CaO catalysts used in biodiesel production has been reported to be similar [13,24,41]. However, when observed under higher magnification, cracks on the surface and sharp edges are visible, which could be useful in exposing strong basic sites but could also cause instability in sintering during the course of the reaction. The EDS spectrum of this image is given in Figure 4c, which shows that the sample is mainly made of calcium and oxygen with no traces of impurities. Even though the EDS spectrum does not give information regarding the oxidation state of the sample, it is clear that the elemental composition of the sample confirms that CaO is synthesized through calcination [35].

The SEM micrograph for $Al_2O_3$-CaO catalyst when observed under a magnification of 1000× and 2500× (Figure 5a,b) shows that there are notable changes in the surface morphology when compared to that of CaO. The Al metal loading was found to be 9.9 wt% for $Al_2O_3$-CaO through EDAX. The observations reveal that the catalyst has a relatively heterogeneous surface morphology when compared to that of CaO. In addition, the surface features are finer when compared to that of CaO. The groups of catalyst particles are also not as thick as those of CaO. This means adding $Al_2O_3$ has a big effect on how CaO changes when heated at high temperatures. This leads to a lot of small surface details spread out across the surface. Also, some of these surface details are covered by a thin layer of areas, which is probably because $Al_2O_3$ is spread out a lot on the catalyst surface. No distinct $Al_2O_3$ phase is visually distinguishable from the SEM micrographs; the phase composition and crystallinity of the catalyst are

discussed based on the XRD results. This SEM result matches with the XRD data analysis. This type of morphology is observed when Ca-O-Al structures are formed, resulting in enhanced catalyst stability without any hindrance on the active sites [29,42]. The EDS spectrum (Figure 5c) confirms that Al is present together with Ca and O, thus proving that impregnation was successful. The EDS elemental mapping indicates a relatively uniform distribution of aluminium across the analyzed catalyst surface.

SEM micrograph of $Fe_2O_3$-CaO base catalyst at 1000× and 2500× magnifications (Figure 6a,b) shows that the catalyst surface is compact and densely packed compared to CaO and $Fe_2O_3$-CaO catalysts. The Fe metal loading was found to be 30.01 wt% for $Fe_2O_3$-CaO through EDAX. The presence of larger clusters of catalyst material with smooth surfaces is also observed, showing strong catalyst particle interactions during calcination. This is commonly associated with strong oxide interactions between CaO and Fe species present in the catalyst material. The surface of $Fe_2O_3$-CaO appears to be partially fused when observed under higher magnification, which could be an indication of some localized sintering effects that could result in smoother surfaces, thus reducing site accessibility. Such catalyst surface evolution is also observed in Fe-modified CaO catalysts, where excessive Fe content leads to crystallite growth and pore coalescence during calcination [30,43].

The spectrum for the SEM EDS (Figure 6c) indicated the existence of iron, calcium, and oxygen. This indicated that the Fe species was incorporated into the catalyst matrix. Even though it was not clear what phase the Fe was in by the use of the EDS analysis tool, it was clear that a mixed metal oxide system was formed, as indicated by the XRD results.

From the results of the SEM-EDS analysis, it was clear that the surface appearance of the eggshell-derived CaO-based catalysts was greatly affected by adding metal oxides. The addition of $Al_2O_3$ influenced the catalyst surface by creating a dispersed surface that could be beneficial for improving the catalyst's activity. On the other hand, the addition of $Fe_2O_3$ influenced the catalyst's surface by creating a more agglomerated surface that could be beneficial for improving the activity by improving interactions of the oxides. This was supported by the trend for the catalyst's activity, which was $Al_2O_3$-CaO > $Fe_2O_3$-CaO > CaO. This indicated that the surface morphology played a greater role than the surface area in improving the biodiesel yield [44,45].

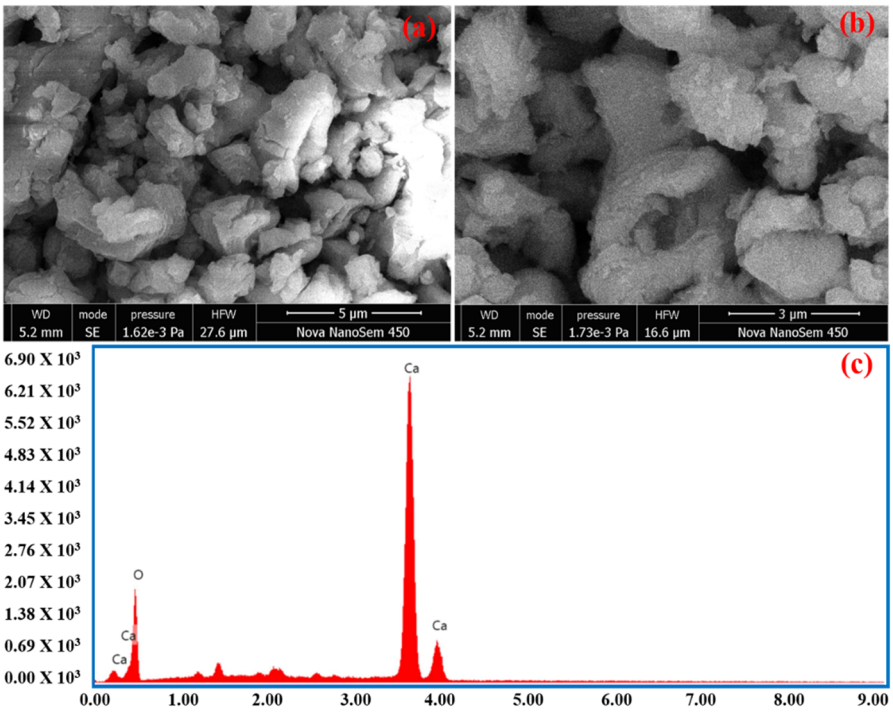


**Figure 4.** SEM-EDS analysis: SEM micrographs of CaO catalyst at different magnifications (**a**,**b**) and corresponding EDS spectrum (**c**) confirming Ca and O as dominant elements.

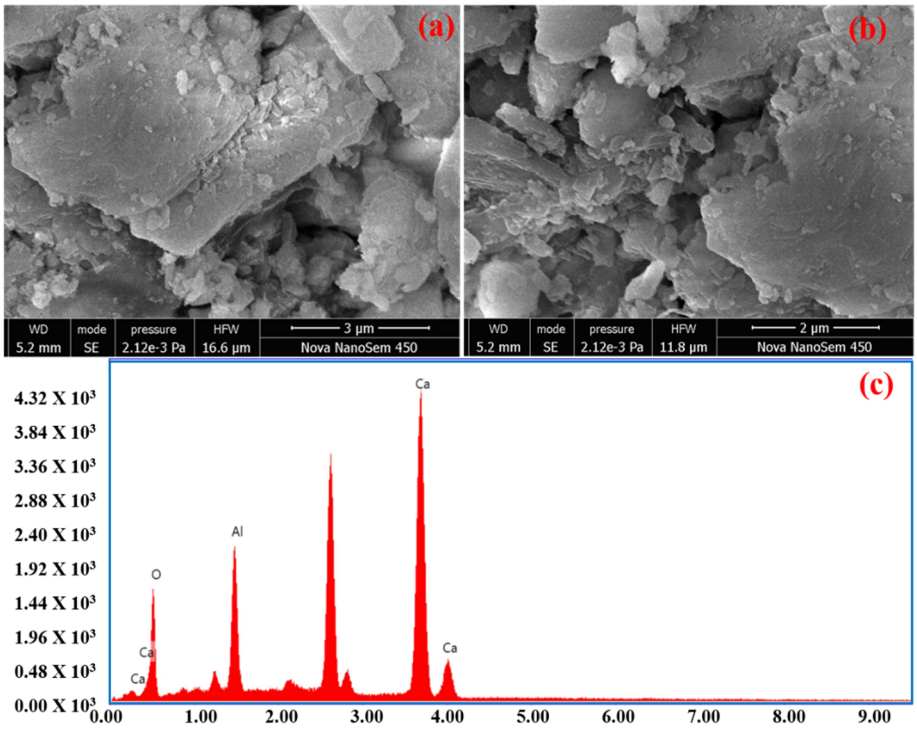


**Figure 5.** SEM-EDS analysis: SEM micrographs of $Al_2O_3$-CaO catalyst (**a**,**b**) showing surface morphology after aluminium impregnation and corresponding EDS spectrum (**c**) confirming successful incorporation of Al.

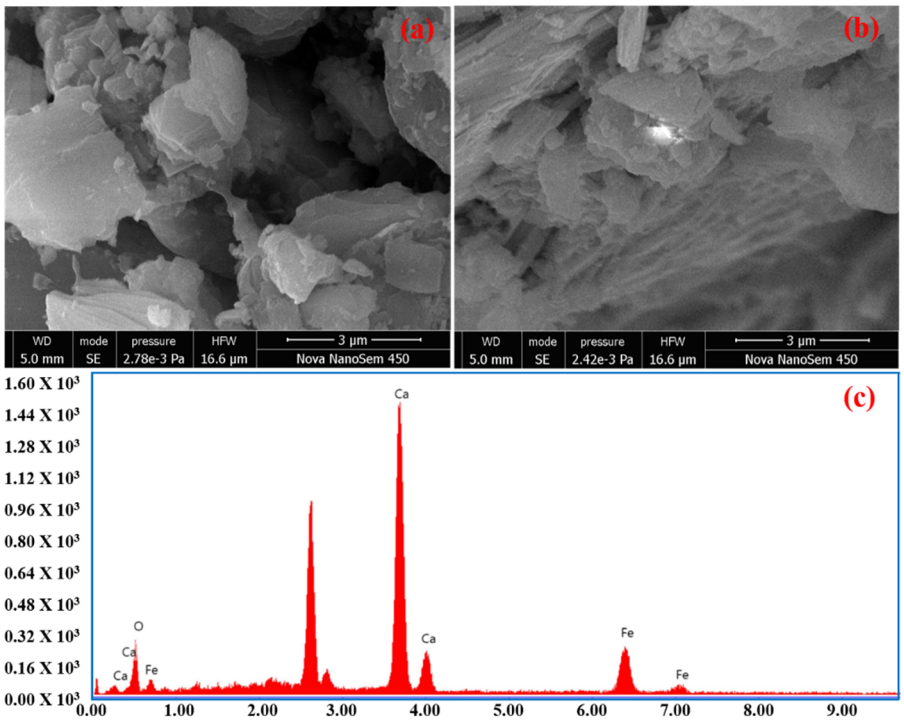


**Figure 6.** SEM-EDS analysis: SEM micrographs of $Fe_2O_3$-CaO catalyst (**a**,**b**) and corresponding EDS spectrum (**c**), indicating substantial Fe incorporation and altered surface morphology.

### *3.4. BET Surface Area and Porosity Analysis*

BET analysis (Figure 7, Tables 2 and 3), it is evident that the surface area is improved progressively after impregnation with metal oxide. CaO surface area without any modifications was 8.82 $m^2$ $g^{-1}$. This result is consistent with the surface area of CaO prepared from eggshells after high-temperature calcination. The surface area of the $Al_2O_3$-CaO catalyst was 4.51 $m^2$ $g^{-1}$ with a moderate increase in the average pore diameters [29,46].

The lowest surface area (2.31 $m^2$ $g^{-1}$) along with the lowest pore volume is observed on the $Fe_2O_3$-CaO catalyst. But the highest value of the average pore diameter (~72 nm) is observed on the $Fe_2O_3$-CaO catalyst. This may be due to the blocking of the pores. From the above results, it can be derived that the improved activity may not be only due to the surface area. The role of surface chemistry may be significant. The pore characteristics are particularly important because transesterification involves relatively bulky triglyceride molecules reacting with methanol in a biphasic reaction medium. Although micropores (<2 nm) may contribute to reactions involving small molecules such as methanol, the accessibility of these pores to triglycerides is expected to be severely restricted by steric and diffusional limitations. Previous studies have demonstrated that the slow diffusion of bulky triglycerides through small pores can limit the utilization of internal catalytic sites, whereas larger mesoporous/macroporous pathways improve reactant accessibility and mass transfer [47]. Therefore, the external surface and larger accessible pores are likely to contribute more strongly to triglyceride conversion than the total BET surface area alone.

In the present study, the reduction in BET surface area after metal-oxide incorporation does not correspond to a reduction in FAME yield. In particular, $Fe_2O_3$-CaO possesses the lowest BET surface area (2.31 $m^2$ $g^{-1}$) but the largest average pore diameter (~72 nm), whereas $Al_2O_3$-CaO exhibits an intermediate surface area (4.51 $m^2$ $g^{-1}$) and achieves the highest FAME yield (94.16%). This observation suggests that BET surface area alone is not the controlling descriptor of catalytic performance; accessible pore structure and surface basic-site characteristics appear to be more important under the investigated conditions.

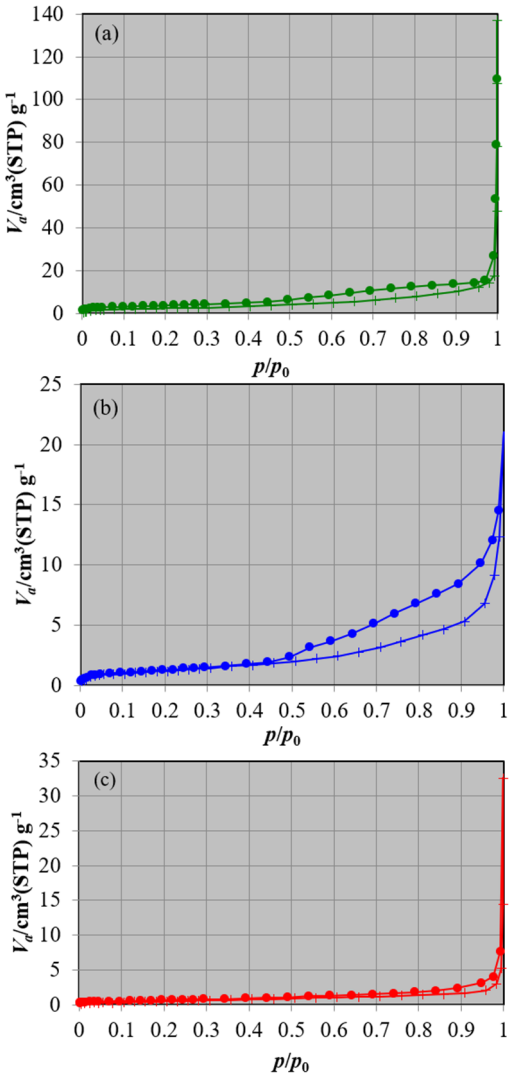


**Figure 7.** Adsorption–desorption isotherms: Nitrogen adsorption–desorption isotherms of (**a**) CaO, (**b**) $Al_2O_3$-CaO, and (**c**) $Fe_2O_3$-CaO catalysts, exhibiting type IV isotherms with H3 hysteresis loops characteristic of mesoporous materials with slit-like pores formed by aggregated plate-like particles.

**Table 2.** BET textural properties: BET surface area, pore volume, and average pore diameter of CaO, $Al_2O_3$/CaO, and $Fe_2O_3$-CaO catalysts derived from nitrogen adsorption–desorption measurements.

| BET Plot Data | CaO | $Al_2O_3$-CaO | $Fe_2O_3$-CaO |
|---|---|---|---|
| $V_m$ [$cm^3$(STP) $g^{-1}$] | 2.0257 | 1.0362 | 0.5311 |
| $a_{s,BETmp}$ [$m^2$ $g^{-1}$] | 8.8168 | 4.51 | 2.3116 |
| Total pore volume ($p/p_0$ = 0.9900) [$cm^3$ $g^{-1}$] | 0.0262 | 0.019 | 0.0066 |
| Average pore diameter (slit) [nm] | 5.9511 | 8.474 | 5.7386 |

**Table 3.** BJH pore characteristics: BJH-derived pore volume and pore diameter parameters of CaO, $Al_2O_3$-CaO, and $Fe_2O_3$-CaO catalysts.

| BJH Plot Data | CaO | $Al_2O_3$/CaO | $Fe_2O_3$/CaO |
|---|---|---|---|
| $V_p$ [$cm^3$ $g^{-1}$] | 0.101 | 0.0267 | 0.0483 |
| $d_{p,peak}$ (Area Vp) [nm] | 1.0454 | 1.0454 | 1.7231 |
| Average pore diameter [nm] | 19.983 | 10.656 | 72.379 |
| Median pore diameter [nm] | 582.35 | 57.786 | 187.26 |

### *3.5. GC-FAME Analysis and Comparison with FAME Standard*

The GC-FAME chromatogram of the biodiesel sample prepared using catalysts derived from eggshell is presented in Figure 8, whereas the result is also tabulated in Table 4. The Gas chromatography of FAME the biodiesel sample is seen to have well-defined peaks within the C16–C18 window. Major FAME components were identified by direct comparison of retention times with those obtained from Supelco FAME certification, Sigma Aldrich, Bangalore, India. Mixture of C4–C24 reference standard was analysed under identical chromatographic conditions. The dominant component was Methyl linolenate (C18:3), followed by Methyl linoleate (C18:2) and Methyl oleate (C18:1). Minor amounts of Methyl docosadienoate (C22:2) and Methyl eicosadienoate (C20:2) were also detected. The high proportion of C18 unsaturated FAMEs is characteristic of biodiesel derived from waste cooking oil and is consistent with previously reported compositions for similar feedstocks, confirming effective conversion and product quality [48].

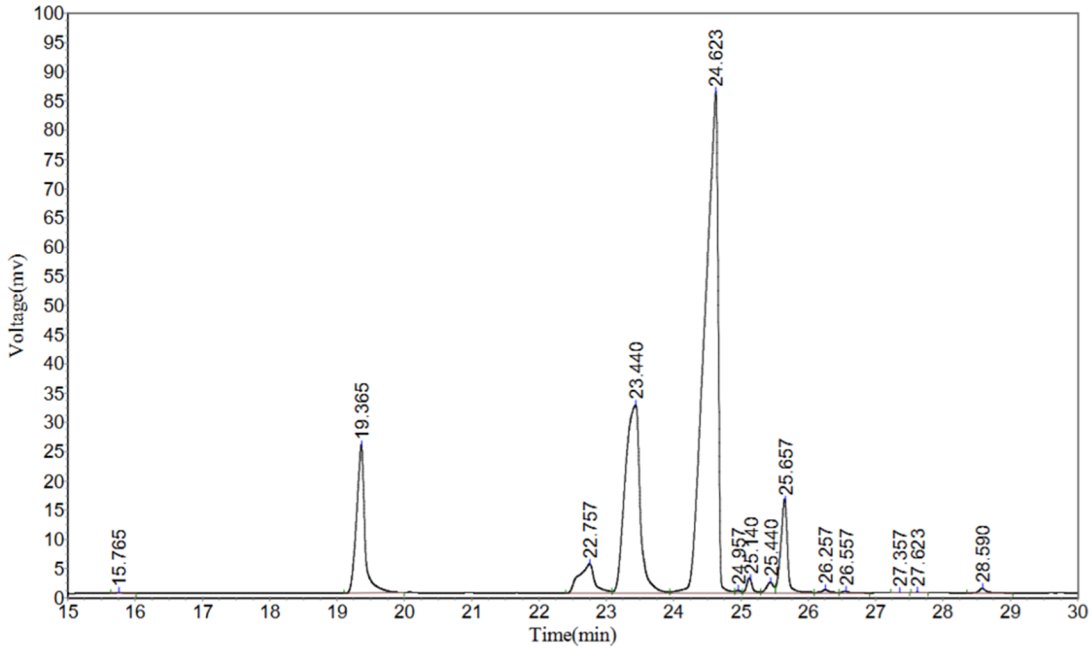


**Figure 8.** GC-FAME chromatogram: Gas chromatographic profile of fatty acid methyl esters produced from waste cooking oil, showing well-resolved peaks within the 15–30 min retention time window consistent with biodiesel components.

**Table 4.** GC-FAME peak assignment: Retention times and corresponding fatty acid methyl ester species identified in biodiesel produced from waste cooking oil.

| Retention Time (min) | Identified FAME | Carbon Chain | Double Bonds | Saturation Type |
|---|---|---|---|---|
| 15.765 | Methyl palmitate | C16:0 | 0 | Saturated |
| 19.365 | Methyl oleate | C18:1 | 1 | Mono-unsaturated |
| 22.757 | Methyl eicosadienoate | C20:2 | 2 | Poly-unsaturated |
| 23.440 | Methyl linoleate | C18:2 | 2 | Polyunsaturated |
| 24.623 | Methyl linolenate | C18:3 | 3 | Polyunsaturated |
| 24.957 | Methyl behenate | C22:0 | 0 | Saturated |
| 25.140 | Methyl behenate/long-chain FAME | C22:0 | 0 | Saturated |
| 25.440 | Methyl erucate | C22:1 | 1 | Mono-unsaturated |
| 25.657 | Methyl docosadienoate | C22:2 | 2 | Poly-unsaturated |
| 26.257 | Methyl eicosatrienoate | C20:3 | 3 | Poly-unsaturated |
| 26.557 | Methyl arachidonate | C20:4 | 4 | Poly-unsaturated |
| 27.357 | Methyl eicosapentaenoate (EPA) | C20:5 | 5 | Poly-unsaturated |
| 27.623 | Methyl nervonate | C24:1 | 1 | Mono-unsaturated |
| 28.590 | Methyl docosahexaenoate (DHA) | C22:6 | 6 | Poly-unsaturated |

### *3.6. Catalytic Performance: FAME Yield Comparison*

The catalytic performance of the prepared eggshell-derived catalysts was evaluated based on FAME yield obtained from the reaction of waste cooking oil under identical, non-optimized transesterification conditions. The unmodified CaO catalyst achieved a FAME yield of 79.46 ± 0.65%, whereas Fe-modified CaO ($Fe_2O_3$-CaO) exhibited an improved yield of 83.98 ± 0.89%. The highest conversion was observed for the Al-modified catalyst ($Al_2O_3$-CaO), which reached a FAME yield of 94.16 ± 0.69%.

The comparatively lower yield of CaO catalyst can be attributed to its high crystalline property which is susceptible to surface carbonation and hydration on exposure to environmental air and moisture. Similar limitations of unmodified CaO catalysts derived from biogenic sources have been widely reported, where partial deactivation of surface basic sites occurs even under controlled reaction conditions [23]. Although CaO inherently provides strong $O^{2-}$ basic sites essential for methanol activation, the reduction in accessible active sites due to moisture and $CO_2$ adsorption can limit overall conversion efficiency [27].

Incorporation of iron oxide into the CaO matrix results in a moderate increase in FAME yield. Even after notable reduction in BET surface area for $Fe_2O_3$-CaO catalyst. It exhibits altered surface chemistry, as evidenced by FTIR and EDS analyses which may contribute to its improved catalytic activity. The presence of Fe-containing species is known to modify the acid-base balance of CaO-based catalysts, potentially enhancing adsorption and activation of methanol and triglyceride molecules at the solid liquid interface [30]. However, extensive pore coalescence and stronger oxide-oxide interactions observed for $Fe_2O_3$-CaO can restrict the effective exposure of strong basic sites, thereby limiting further improvement in yield [49].

Among the three catalysts, $Al_2O_3$-CaO demonstrates the highest catalytic performance. Although its BET surface area is lower than that of unmodified CaO, aluminium modification appears to stabilize CaO surface basic sites and mitigate deactivation pathways [50]. The absence of distinct crystalline $Al_2O_3$ peaks in XRD suggests that aluminium oxide is highly dispersed, likely forming Ca-O-Al interfacial linkages that enhance catalytic efficiency without severely blocking active sites. Similar enhancements in biodiesel yield for $Fe_2O_3$-CaO systems have been attributed to improved surface stability and preservation of strong basic sites rather than surface area enhancement [51,52].

Significantly, the observed trend for the catalysts' activity ($Al_2O_3$-CaO > $Fe_2O_3$-CaO > CaO) does not follow any specific trend related to textural properties and supports the results obtained by recent publications of great scientific impact regarding the fact that surface chemistry and quality of basic sites of CaO-based catalysts for transesterification are more important than textural properties [53,54]. The results obtained using FTIR, XRD, BET, and EDS techniques suggest that the impregnation of metal oxide plays crucial performance regarding surface parameters and stability while preserving the backbone of CaO catalysts for non-optimized conditions.

### *3.7. Catalyst Reusability*

Consistent decrease in the biodiesel production was examined for all catalyst systems with increasing reuse cycles. The unmodified CaO catalyst exhibited the most pronounced loss in catalytic activity, with FAME yield decreasing from 79.46 ± 0.65% in the first cycle to 56.91 ± 1.28% after the 5th cycle. This corresponds to a loss of approximately 28.38% of its initial activity. The reduction in production might be due to leaching of the active

Ca ion in reaction medium, blockage of catalytic sites by adsorbed organic compounds, and partial surface carbonation or hydration during repeated use [55,56].

The $Fe_2O_3$-CaO catalyst demonstrated improved operational stability compared with pristine CaO. The FAME yield decreased from 83.98 ± 0.89% in the first cycle to 68.96 ± 1.19% in the fifth cycle, indicating a lower rate of deactivation. The enhanced stability is likely associated with the interaction between iron oxide and the CaO support, which may reduce active phase loss and improve structural integrity during repeated transesterification reactions [57,58].

Among all catalysts, $Al_2O_3$-CaO exhibited the highest reusability and retained superior catalytic performance throughout the study. The catalyst maintained a FAME yield of 85.76 ± 0.89% after five cycles compared with an initial yield of 94.16 ± 0.69%, corresponding to a retention of approximately 91.08% of its original activity. The improved durability may be attributed to the strong interaction between $Al_2O_3$ and CaO, which enhances catalyst stability, suppresses active-site leaching, and minimizes surface deactivation caused by deposition of reaction by-products [36,42].

This trend confirms that metal oxide modification significantly enhances the long-term stability of eggshell-derived CaO catalysts. The superior performance of $Al_2O_3$-CaO suggests that alumina modification not only improves catalytic activity but also provides greater resistance to deactivation during repeated biodiesel production cycles, making it a promising catalyst for practical and economically viable biodiesel synthesis. The FAME yields obtained over five consecutive transesterification cycles for all three catalyst systems are summarised in Table 5 and Figure 9, demonstrating the superior reusability and catalytic stability of $Al_2O_3$-CaO compared with pristine CaO and $Fe_2O_3$-CaO. A comparison of the catalytic performance of the present eggshell-derived CaO-based catalysts with previously reported heterogeneous catalysts is provided in Table 6. Unlike many reported systems evaluated under individually optimized reaction conditions, the present catalysts were comparatively assessed under identical non-optimised conditions using multiple-frying waste cooking oil, enabling a more direct evaluation of the influence of $Al_2O_3$ and $Fe_2O_3$ incorporation on catalytic performance.

**Table 5.** Reusability performance (in terms of % FAME yield) of eggshell derived catalysts over five consecutive transesterification cycles.

| Cycle No. | CaO (%FAME) | $Fe_2O_3$-CaO (%FAME) | $Al_2O_3$-CaO (%FAME) |
|---|---|---|---|
| 1 | 79.46 ± 0.65 | 83.98 ± 0.89 | 94.16 ± 0.69 |
| 2 | 73.90 ± 0.99 | 80.92 ± 0.79 | 92.38 ± 0.59 |
| 3 | 68.07 ± 1.19 | 77.16 ± 1.09 | 90.11 ± 0.89 |
| 4 | 63.33 ± 0.79 | 72.91 ± 0.99 | 87.93 ± 0.79 |
| 5 | 56.91 ± 1.28 | 68.96 ± 1.19 | 85.76 ± 0.89 |

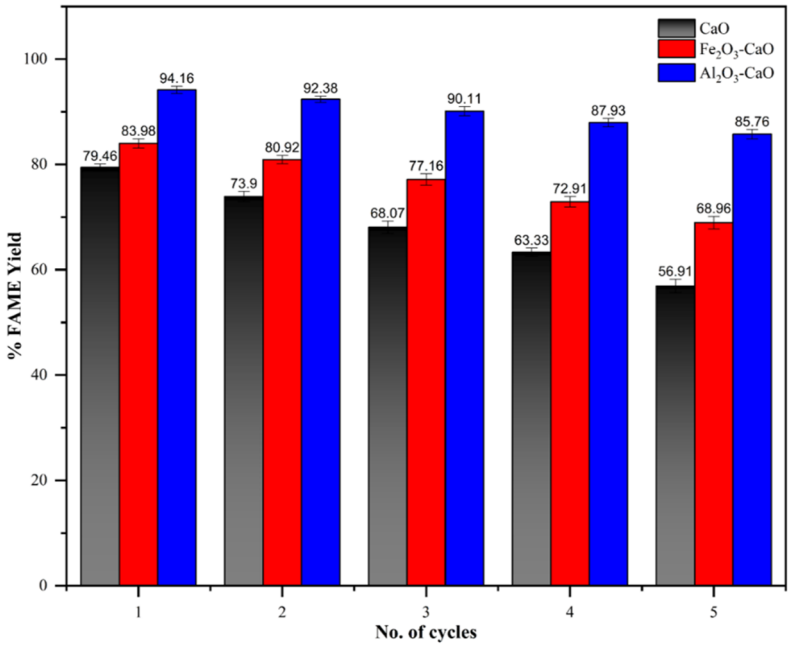


**Figure 9.** Reusability of unmodified CaO, $Fe_2O_3$-CaO and $Al_2O_3$-CaO catalysts for transesterification of multiple-frying waste cooking oil. % FAME yield obtained over five consecutive reaction cycles.

**Table 6.** Comparative catalytic performance of heterogeneous catalysts reported for FAME yield.

| Heterogeneous Catalyst | Feedstock<br>Methanol:Oil<br>Catalyst Loading,<br>Temperature<br>Reaction Time | FAME Yield |
|---|---|---|
| Modified red mud (soda-lime calcined) [59] | Canola oil<br>12:1<br>4 wt%<br>60 °C<br>2 h | >99% |
| $K_2CO_3$/red-mud composite (KRM) [60] | Castor oil<br>18:1<br>5 wt%<br>65 °C<br>2.5 h | 94.52% |
| KOH/$Al_2O_3$ [61] | Palm oil<br>15:1<br>3–6 wt%<br><70 °C<br>2–3 h | 91.07% |
| CaO/$Al_2O_3$ [26] | Palm oil<br>—<br>Optimized<br>Moderate<br>— | 94% |
| CaO/neutral-$Al_2O_3$ [36] | Soybean oil<br>—<br>20 wt% CaO<br>150 °C<br>1 h | 90% |
| $Al_2O_3$–eggshell catalyst [28] | Spent vegetable oil<br>—<br>1 wt%<br>90 °C<br>120 min | 94.23 ± 0.50% |
| $Fe_2O_3$–eggshell catalyst [28] | Spent vegetable oil<br>—<br>1 wt%<br>90 °C<br>120 min | 91.94 ± 0.21% |
| Rice-husk-derived sodium silicate [62] | Vegetable oils<br>12:1<br>2.5 wt%<br>65 °C<br>30 min | 97% FAME |
| Sugarcane-leaf-derived $SiO_2$ xerogel [63] | Canola oil<br>6:1<br>3 wt%<br>65 °C<br>60 min | 96.9% |
| CaO derived from waste mussel shell [64] | Palm oil<br>9:1<br>10 wt%<br>65 °C<br>3–4 h | 97.23% |
| CaO derived from waste cockle shell [64] | Palm oil<br>9:1<br>10 wt%<br>65 °C<br>3–4 h | 94.47% |
| Eggshell-derived CaDG [25] | Waste cooking oil<br>10:1<br>1.5 wt%<br>60 °C<br>50 min | 96.07% |

**Table 6.** *Cont.*

| Heterogeneous Catalyst | Feedstock<br>Methanol:Oil<br>Catalyst Loading,<br>Temperature<br>Reaction Time | FAME Yield |
|---|---|---|
| $CaO/Al_2O_3$ pellet [29] | Palm oil<br>12:1<br>10 wt%<br>65 °C<br>6 h | 78.7% |
| K-$CaO/Al_2O_3$ pellet [29] | Palm oil<br>12:1<br>10 wt%<br>65 °C<br>6 h | 88.8% |
| Present study: eggshell-CaO | Multiple-frying WCO<br>8:1<br>4 wt%<br>65 °C<br>180 min | 79.46 ± 0.65% |
| Present study: $Fe_2O_3/CaO$ | Multiple-frying WCO<br>8:1<br>4 wt%<br>65 °C<br>180 min | 83.98 ± 0.89% |
| Present study: $Al_2O_3/CaO$ | Multiple-frying WCO<br>8:1<br>4 wt%<br>65 °C<br>180 min | 94.16 ± 0.69% |

## 4. Discussion

CaO, and $Al_2O_3$-CaO, $Fe_2O_3$-CaO catalytic property, can be explained on the basis of its surface chemistry as well as surface access, as opposed to surface area only. Moreover, CaO is a well-examined heterogeneous base catalyst responsible for the transesterification reaction. Its actual efficiency of transesterification is often restricted due to its rapid surface carbonation, hydration, as well as leaching, especially when derived from biogenic $CaCO_3$ [17,65]. The existence of hydroxyl groups and $CO_3$ on the catalyst surfaces is also verified using the FTIR technique. This confirms that it is not easy to remove the CaO reactivity on the catalyst surfaces toward $CO_2$ and moisture under ambient handling conditions. The catalysts have different vibrational modes of metal oxygen species. This confirms the modification of the CaO surfaces is due to the impregnation of Al ion and Fe ion. Which affects the efficacy of the basic sites. Very important in methanol activation during transesterification [66].

The trend is also confirmed by the XRD data, where CaO alone has distinct peaks indicating large domains of well-ordered material. The $Al_2O_3$-CaO composite retains the CaO phase but has lower peak height and some broadening of peaks, indicating better dispersion or lattice distortion in the absence of $Al_2O_3$ crystallites. In contrast, $Fe_2O_3$-CaO shows additional diffraction features associated with iron oxide related phases, indicating stronger interactions between oxides and partial restructuring of the CaO matrix. Similar behaviour has been reported for $Al_2O_3$-CaO catalyst, where mixed or interfacial phases influence catalytic behaviour but may also limit accessibility of CaO basic sites [67,68]. BET analysis reveals that surface area decreases progressively upon metal oxide impregnation, with $Fe_2O_3$-CaO exhibiting the lowest surface area and largest average pore diameter. This indicates pore coalescence or partial structural collapse during high temperature calcination, particularly in the presence of iron species. Importantly, the highest FAME yield is not associated with the highest surface area, reinforcing the notion that basic site quality and surface stability outweigh textural parameters in CaO based transesterification catalysts [69]. The superior performance of the $Al_2O_3$-CaO catalyst (94.16% FAME yield) can therefore be attributed to a more favourable balance between surface modification and site accessibility. Aluminium oxide appears to act as a stabilizing phase, limiting CaO sintering and surface deactivation while remaining sufficiently dispersed to avoid severe pore blockage. The development of Ca-O-Al interfacial sites has been reported to enhance the resistance to carbonation and longevity of the catalysts in similar systems [70,71].

In comparison to Fe-modified CaO and CaO, Al-modified CaO, Al-modified CaO is showing better performance. Moreover Fe-CaO is showing better performance in comparison to CaO. So, that the moderate catalytic performance of $Fe_2O_3$-CaO systems, despite the changes in the surface chemistry. Similar trends have

been observed for other CaO-based catalysts prepared from mixed CaO-oxide systems, wherein overloading of secondary oxide phases has shown diminishing returns [72]. The trend in catalyst performance: $Al_2O_3$-CaO > $Fe_2O_3$-CaO > CaO is likely related to a structure-activity relationship where surface stabilization is predominantly relevant, rather than surface area development or phase transformation.

Overall, the results show that simple oxide modification of waste-derived CaO can substantially improve catalytic performance and reusability without changing the underlying low-cost calcium-based catalyst platform. This provides a practical route for valorizing eggshell waste while simultaneously utilizing waste cooking oil for biodiesel production. However, the present study was designed as a comparative evaluation rather than a systematic optimization of metal loading, calcination conditions, or reaction parameters. Moreover, catalyst deactivation mechanisms and the exact nature of the modified/interfacial phases were not directly verified through post-reaction characterization or elemental leaching measurements. Further studies involving optimization of oxide loading, basicity measurements, Ca-leaching analysis, and post-reaction structural characterization are therefore recommended to establish the structure–activity–stability relationships more conclusively.

## Author Contributions

R.Y.: Conceptualization, experimental investigation, methodology, investigation, formal analysis, data curation, writing original draft; K.P.: Sample preparation, characterization, data acquisition, validation; S.N.: Literature review, visualization, data interpretation, manuscript preparation; A.K.: Experimental investigation, data validation, review and editing; A.M.: Supervision, research planning, resource acquisition, review and editing. All authors have read and agreed to the published version of the manuscript.

## Funding

This research received no external funding.

## Institutional Review Board Statement

Not applicable.

## Informed Consent Statement

Not applicable.

## Data Availability Statement

The data supporting the findings of this study are available from the corresponding author upon reasonable request. The raw experimental data and relevant supporting information will be made available to qualified researchers, subject to reasonable requests and applicable institutional policies.

## Acknowledgments

The authors are thankful to the School of Biochemical Engineering, IIT (BHU) for providing necessary facilities to carry out the present research work. The authors are also thankful to the Central Instrumentation Facility, IIT (BHU) for providing facilities for XRD analysis, HR-SEM analysis, EDS analysis, BET analysis. Authors sincerely acknowledges the financial support from the CSIR-New Delhi, India and MHRD, Government of India.

## Conflicts of Interest

The authors declare no conflict of interest.

## Use of AI and AI-Assisted Technologies

No AI tools were utilized for this paper.

## References

1. Ahmed, R.A.; Huddersman, K. Short Review of Biodiesel Production by the Esterification/Transesterification of Wastewater Containing Fats Oils and Grease (FOGs). In *Energy and Sustainable Futures: Proceedings of the 3rd ICESF, 2022*; Nixon,

J.D., Al-Habaibeh, A., Vukovic, V. et al., eds.; Springer Nature Switzerland: Cham, Switzerland, 2023; pp. 285–299. https://doi.org/10.1007/978-3-031-30960-1_27.

2. Beghetto, V. Waste Cooking Oils into High-Value Products: Where Is the Industry Going? *Polymers* **2025**, *17*, 887. https://doi.org/10.3390/polym17070887.
3. Khan, M.A.; Sheikh, N.A.; Jadoon, K.Z.; et al. Utilization of locally sourced waste fats for biodiesel production: Experimental characterization and environmental life cycle assessment. *Biomass Bioenergy* **2025**, *194*, 107692. https://doi.org/10.1016/j.biombioe.2025.107692.
4. Chai, M.; Tu, Q.; Lu, M.; et al. Esterification pretreatment of free fatty acid in biodiesel production, from laboratory to industry. *Fuel Process. Technol.* **2014**, *125*, 106–113. https://doi.org/10.1016/j.fuproc.2014.03.025.
5. Vural Gürsel, I.; Noël, T.; Wang, Q.; et al. Separation/recycling methods for homogeneous transition metal catalysts in continuous flow. *Green Chem.* **2015**, *17*, 2012–2026. https://doi.org/10.1039/c4gc02160f.
6. Vicente, G.; Martínez, M.; Aracil, J. Integrated biodiesel production: A comparison of different homogeneous catalysts systems. *Bioresour. Technol.* **2004**, *92*, 297–305. https://doi.org/10.1016/j.biortech.2003.08.014.
7. Colombo, K.; Ender, L.; Barros, A.A.C. The study of biodiesel production using CaO as a heterogeneous catalytic reaction. *Egypt. J. Pet.* **2017**, *26*, 341–349. https://doi.org/10.1016/j.ejpe.2016.05.006.
8. Tang, Y.; Xu, J.; Zhang, J.; et al. Biodiesel production from vegetable oil by using modified CaO as solid basic catalysts. *J. Clean. Prod.* **2013**, *42*, 198–203. https://doi.org/10.1016/j.jclepro.2012.11.001.
9. Ayodeji, A.A.; Modupe, O.E.; Rasheed, B.; et al. Data on CaO and eggshell catalysts used for biodiesel production. *Data Brief* **2018**, *19*, 1466–1473. https://doi.org/10.1016/j.dib.2018.06.028.
10. Sierra-Cantor, J.F.; Parra-Santiago, J.J.; Guerrero-Fajardo, C.A. Leaching and reusing analysis of calcium–zinc mixed oxides as heterogeneous catalysts in the biodiesel production from refined palm oil. *Int. J. Environ. Sci. Technol.* **2019**, *16*, 643–654. https://doi.org/10.1007/s13762-018-1710-2.
11. Mahesh, S.E.; Ramanathan, A.; Begum, K.M.M.S.; et al. Biodiesel production from waste cooking oil using KBr impregnated CaO as catalyst. *Energy Convers. Manag.* **2015**, *91*, 442–450. https://doi.org/10.1016/j.enconman.2014.12.031.
12. Kaur, M.; Ali, A. Lithium ion impregnated calcium oxide as nano catalyst for the biodiesel production from karanja and jatropha oils. *Renew. Energy* **2011**, *36*, 2866–2871. https://doi.org/10.1016/j.renene.2011.04.014.
13. Kumar, D.; Ali, A. Transesterification of Low-Quality Triglycerides over a Zn/CaO Heterogeneous Catalyst: Kinetics and Reusability Studies. *Energy Fuels* **2013**, *27*, 3758–3768. https://doi.org/10.1021/ef400594t.
14. Kaur, N.; Ali, A. Kinetics and reusability of Zr/CaO as heterogeneous catalyst for the ethanolysis and methanolysis of *Jatropha curcas* oil. *Fuel Process. Technol.* **2014**, *119*, 173–184. https://doi.org/10.1016/j.fuproc.2013.11.002.
15. McVicker, G. Surface area stabilization of $Ir/Al_2O_3$ catalysts by CaO, SrO, and BaO under oxygen atmospheres: Implications on the mechanism of catalyst sintering and redispersion. *J. Catal.* **1978**, *54*, 129–142. https://doi.org/10.1016/0021-9517(78)90036-2.
16. Liu, Q.; Xin, R.; Li, C.; et al. Application of red mud as a basic catalyst for biodiesel production. *J. Environ. Sci.* **2013**, *25*, 823–829. https://doi.org/10.1016/s1001-0742(12)60067-9.
17. Dias, A.P.S.; Ramos, M. On the storage stability of CaO biodiesel catalyst. Hydration and carbonation poisoning. *J. Environ. Chem. Eng.* **2021**, *9*, 104917. https://doi.org/10.1016/j.jece.2020.104917.
18. Wei, Z.; Xu, C.; Li, B. Application of waste eggshell as low-cost solid catalyst for biodiesel production. *Bioresour. Technol.* **2009**, *100*, 2883–2885. https://doi.org/10.1016/j.biortech.2008.12.039.
19. El-Sherif, A.A.; Hamad, A.M.; Shams-Eldin, E.; et al. Power of recycling waste cooking oil into biodiesel via green CaO-based eggshells/Ag heterogeneous nanocatalyst. *Renew. Energy* **2023**, *202*, 1412–1423. https://doi.org/10.1016/j.renene.2022.12.041.
20. Macheli, L.; Leteba, G.M.; George, S.L.; et al. Enhancing waste eggshell-derived CaO catalysts for biodiesel production through synergistic oxide modification: A comprehensive catalytic and kinetic study. *RSC Adv.* **2026**, *16*, 5990–6001. https://doi.org/10.1039/d5ra06382e.
21. Rahman, W.U.; Khan, R.I.A.; Ahmad, S.; et al. Valorizing waste palm oil towards biodiesel production using calcareous eggshell based heterogeneous catalyst. *Bioresour. Technol. Rep.* **2023**, *23*, 101584. https://doi.org/10.1016/j.biteb.2023.101584.
22. Falowo, O.A.; Ojediran, O.J.; Moses, O.; et al. A bifunctional catalyst from waste eggshells and its application in biodiesel synthesis from waste cooking oil. *Results Eng.* **2024**, *23*, 102613. https://doi.org/10.1016/j.rineng.2024.102613.
23. Kouzu, M.; Hidaka, J.S. Transesterification of vegetable oil into biodiesel catalyzed by CaO: A review. *Fuel* **2012**, *93*, 1–12. https://doi.org/10.1016/j.fuel.2011.09.015.
24. Erchamo, Y.S.; Mamo, T.T.; Workneh, G.A.; et al. Improved biodiesel production from waste cooking oil with mixed methanol–ethanol using enhanced eggshell-derived CaO nano-catalyst. *Sci. Rep.* **2021**, *11*, 6708. https://doi.org/10.1038/s41598-021-86062-z.
25. Gupta, A.R.; Rathod, V.K. Waste cooking oil and waste chicken eggshells derived solid base catalyst for the biodiesel production: Optimization and kinetics. *Waste Manag.* **2018**, *79*, 169–178. https://doi.org/10.1016/j.wasman.2018.07.022.

26. Zabeti, M.; Daud, W.M.A.W.; Aroua, M.K. Optimization of the activity of $CaO/Al_2O_3$ catalyst for biodiesel production using response surface methodology. *Appl. Catal. A Gen.* **2009**, *366*, 154–159. https://doi.org/10.1016/j.apcata.2009.06.047.
27. Abusweireh, R.S.; Rajamohan, N.; Vasseghian, Y. Enhanced production of biodiesel using nanomaterials: A detailed review on the mechanism and influencing factors. *Fuel* **2022**, *319*, 123862. https://doi.org/10.1016/j.fuel.2022.123862.
28. Abati, S.M.; Bamisaye, A.; Adaramaja, A.A.; et al. Biodiesel production from spent vegetable oil with $Al_2O_3$ and $Fe_2O_3$-biobased heterogenous nanocatalysts: Comparative and optimization studies. *Fuel* **2024**, *364*, 130847. https://doi.org/10.1016/j.fuel.2023.130847.
29. Chanthon, N.; Munbupphachart, N.; Ngaosuwan, K.; et al. Metal loading on $CaO/Al_2O_3$ pellet catalyst as a booster for transesterification in biodiesel production. *Renew. Energy* **2023**, *218*, 119336. https://doi.org/10.1016/j.renene.2023.119336.
30. Ezzah-Mahmudah, S.; Lokman, I.M.; Saiman, M.I.; et al. Synthesis and characterization of $Fe_2O_3$/CaO derived from *Anadara granosa* for methyl ester production. *Energy Convers. Manag.* **2016**, *126*, 124–131. https://doi.org/10.1016/j.enconman.2016.07.072.
31. Lu, J.; Khot, S.; Wool, R.P. New sheet molding compound resins from soybean oil. I. Synthesis and characterization. *Polymer* **2005**, *46*, 71–80. https://doi.org/10.1016/j.polymer.2004.10.060.
32. Chavan, S.B.; Kumbhar, R.R.; Madhu, D.; et al. Synthesis of biodiesel from *Jatropha curcas* oil using waste eggshell and study of its fuel properties. *RSC Adv.* **2015**, *5*, 63596–63604. https://doi.org/10.1039/c5ra06937h.
33. Dissanayake, T.T.; Crawford-Clark, S.; Bowen, B.J.; et al. Comparison of Methods for the Preparation of Fatty Acid Methyl Esters for the Analysis of Omega-3 Rich Oils by Gas Chromatography. *J. Am. Oil Chem. Soc.* **2025**, *102*, 1351–1361. https://doi.org/10.1002/aocs.12974.
34. Kouzu, M.; Kasuno, T.; Tajika, M.; et al. Calcium oxide as a solid base catalyst for transesterification of soybean oil and its application to biodiesel production. *Fuel* **2008**, *87*, 2798–2806. https://doi.org/10.1016/j.fuel.2007.10.019.
35. Abu-Ghazala, A.H.; Abdelhady, H.H.; Mazhar, A.A.; et al. Exceptional room temperature catalytic transesterification of waste cooking oil to biodiesel using environmentally-benign $K_2CO_3/\gamma$-$Al_2O_3$ nano-catalyst. *Chem. Eng. J.* **2023**, *474*, 145784. https://doi.org/10.1016/j.cej.2023.145784.
36. Pasupulety, N.; Gunda, K.; Liu, Y.; et al. Production of biodiesel from soybean oil on $CaO/Al_2O_3$ solid base catalysts. *Appl. Catal. A Gen.* **2013**, *452*, 189–202. https://doi.org/10.1016/j.apcata.2012.10.006.
37. Wu, S.F.; Li, Q.H.; Kim, J.N.; et al. Properties of a Nano $CaO/Al_2O_3$ $CO_2$ Sorbent. *Ind. Eng. Chem. Res.* **2008**, *47*, 180–184. https://doi.org/10.1021/ie0704748.
38. Liu, X.; He, H.; Wang, Y.; et al. Transesterification of soybean oil to biodiesel using CaO as a solid base catalyst. *Fuel* **2008**, *87*, 216–221. https://doi.org/10.1016/j.fuel.2007.04.013.
39. Tian, Y.; Pan, X.; Yu, H.; et al. Formation mechanism of calcium aluminate compounds based on high-temperature solid-state reaction. *J. Alloys Compd.* **2016**, *670*, 96–104. https://doi.org/10.1016/j.jallcom.2016.02.059.
40. Antunes, I.; Ruivo, L.C.M.; Tarelho, L.A.C.; et al. Solid state synthesis of $Ca_2Fe_2O_5$ by reactive firing of calcite and siderite. *Ceram. Int.* **2022**, *48*, 34025–34032. https://doi.org/10.1016/j.ceramint.2022.08.002.
41. Widayat, W.; Darmawan, T.; Hadiyanto, H.; et al. Preparation of Heterogeneous CaO Catalysts for Biodiesel Production. *J. Phys. Conf. Ser.* **2017**, *877*, 012018. https://doi.org/10.1088/1742-6596/877/1/012018.
42. Marinković, D.M.; Avramović, J.M.; Stanković, M.V.; et al. Synthesis and characterization of spherically-shaped $CaO/\gamma$-$Al_2O_3$ catalyst and its application in biodiesel production. *Energy Convers. Manag.* **2017**, *144*, 399–413. https://doi.org/10.1016/j.enconman.2017.04.079.
43. Shi, M.; Zhang, P.; Fan, M.; et al. Influence of crystal of $Fe_2O_3$ in magnetism and activity of nanoparticle $CaO@Fe_2O_3$ for biodiesel production. *Fuel* **2017**, *197*, 343–347. https://doi.org/10.1016/j.fuel.2017.02.060.
44. Kocík, J.; Hájek, M.; Troppová, I. The factors influencing stability of Ca–Al mixed oxides as a possible catalyst for biodiesel production. *Fuel Process. Technol.* **2015**, *134*, 297–302. https://doi.org/10.1016/j.fuproc.2015.02.013.
45. Mohd Kamal, N.; Wan Abu Bakar, W.A.; Ali, R. Catalytic optimization and physicochemical studies over $Zn/Ca/Al_2O_3$ catalyst for transesterification of low grade cooking oil. *Energy Convers. Manag.* **2017**, *137*, 113–120. https://doi.org/10.1016/j.enconman.2017.01.037.
46. Saupsor, J.; Wongsakulphasatch, S.; Kim-Lohsoontorn, P.; et al. $Fe_2O_3/CaO$-$Al_2O_3$ multifunctional catalyst for hydrogen production by sorption-enhanced chemical looping reforming of ethanol. *Biomass Convers. Biorefin.* **2023**, *13*, 8651–8668. https://doi.org/10.1007/s13399-020-00947-z.
47. Witoon, T.; Bumrungsalee, S.; Vathavanichkul, P.; et al. Biodiesel production from transesterification of palm oil with methanol over CaO supported on bimodal meso-macroporous silica catalyst. *Bioresour. Technol.* **2014**, *156*, 329–334. https://doi.org/10.1016/j.biortech.2014.01.076.
48. Torres, A.; Fuentes, B.; Rodríguez, K.E.; et al. Analysis of the Content of Fatty Acid Methyl Esters in Biodiesel by Fourier-Transform Infrared Spectroscopy: Method and Comparison with Gas Chromatography. *J. Am. Oil Chem. Soc.* **2020**, *97*, 651–661. https://doi.org/10.1002/aocs.12350.

49. Hu, M.; Pu, J.; Qian, E.W.; et al. Biodiesel Production Using MgO–CaO Catalysts via Transesterification of Soybean Oil: Effect of MgO Addition and Insights of Catalyst Deactivation. *BioEnergy Res.* **2023**, *16*, 2398–2410. https://doi.org/10.1007/s12155-023-10580-z.
50. Moradi, G.; Mohadesi, M.; Rezaei, R.; et al. Biodiesel Production using CaO/γ-$Al_2O_3$ Catalyst Synthesized by Sol-Gel Method. *Can. J. Chem. Eng.* **2015**, *93*, 1531–1538. https://doi.org/10.1002/cjce.22258.
51. Kingkam, W.; Nuchdang, S.; Phalakornkule, C.; et al. Synergistic effect of $La_2O_3$-$Al_2O_3$ based catalysts for efficient biodiesel production. *J. Ind. Eng. Chem.* **2025**, *143*, 197–212. https://doi.org/10.1016/j.jiec.2024.08.023.
52. Taufiq-Yap, Y.H.; Lee, H.V.; Hussein, M.Z.; et al. Calcium-based mixed oxide catalysts for methanolysis of *Jatropha curcas* oil to biodiesel. *Biomass Bioenergy* **2011**, *35*, 827–834. https://doi.org/10.1016/j.biombioe.2010.11.011.
53. Pandit, P.R.; Fulekar, M.H. Biodiesel production from microalgal biomass using CaO catalyst synthesized from natural waste material. *Renew. Energy* **2019**, *136*, 837–845. https://doi.org/10.1016/j.renene.2019.01.047.
54. Sulaiman, N.F.; Ramly, N.I.; Abd Mubin, M.H.; et al. Transition metal oxide (NiO, CuO, ZnO)-doped calcium oxide catalysts derived from eggshells for the transesterification of refined waste cooking oil. *RSC Adv.* **2021**, *11*, 21781–21795. https://doi.org/10.1039/d1ra02076e.
55. Oueda, N.; Bonzi-Coulibaly, Y.L.; Ouédraogo, I.W.K. Deactivation Processes, Regeneration Conditions and Reusability Performance of CaO or MgO Based Catalysts Used for Biodiesel Production—A Review. *Mater. Sci. Appl.* **2017**, *8*, 94–122. https://doi.org/10.4236/msa.2017.81007.
56. Li, H.; Wang, Y.; Ma, X.; et al. A novel magnetic CaO-based catalyst synthesis and characterization: Enhancing the catalytic activity and stability of CaO for biodiesel production. *Chem. Eng. J.* **2020**, *391*, 123549. https://doi.org/10.1016/j.cej.2019.123549.
57. Helwani, Z.; Ramli, M.; Saputra, E.; et al. Impregnation of CaO from Eggshell Waste with Magnetite as a Solid Catalyst ($Fe_3O_4$/CaO) for Transesterification of Palm Oil Off-Grade. *Catalysts* **2020**, *10*, 164. https://doi.org/10.3390/catal10020164.
58. Ali, M.A.; Al-Hydary, I.A.; Al-Hattab, T.A. Nano-Magnetic Catalyst CaO-$Fe_3O_4$ for Biodiesel Production from Date Palm Seed Oil. *Bull. Chem. React. Eng. Catal.* **2017**, *12*, 460–468. https://doi.org/10.9767/bcrec.12.3.923.460-468.
59. Wahyudi, A.; Kurniawan, W.; Hinode, H. Utilization of Modified Red Mud as a Heterogeneous Base Catalyst for Transesterification of Canola Oil. *J. Chem. Eng. Jpn.* **2017**, *50*, 561–567. https://doi.org/10.1252/jcej.16we337.
60. Liu, K.; Wei, G.; Zhu, Y.; et al. A clean route of biodiesel production using red mud-based potassium catalyst. *J. Environ. Chem. Eng.* **2023**, *11*, 111015. https://doi.org/10.1016/j.jece.2023.111015.
61. Noiroj, K.; Intarapong, P.; Luengnaruemitchai, A.; et al. A comparative study of KOH/$Al_2O_3$ and KOH/NaY catalysts for biodiesel production via transesterification from palm oil. *Renew. Energy* **2009**, *34*, 1145–1150. https://doi.org/10.1016/j.renene.2008.06.015.
62. Roschat, W.; Siritanon, T.; Yoosuk, B.; et al. Rice husk-derived sodium silicate as a highly efficient and low-cost basic heterogeneous catalyst for biodiesel production. *Energy Convers. Manag.* **2016**, *119*, 453–462. https://doi.org/10.1016/j.enconman.2016.04.071.
63. Maseko, N.N.; Enke, D.; Owolawi, P.A.; et al. Usage of Silica Xerogel from African Sugarcane Leaves as a Catalyst in Biodiesel Production through Transesterification. *ACS Omega* **2025**, *10*, 28032–28042. https://doi.org/10.1021/acsomega.5c01971.
64. Buasri, A.; Chaiyut, N.; Loryuenyong, V.; et al. Calcium Oxide Derived from Waste Shells of Mussel, Cockle, and Scallop as the Heterogeneous Catalyst for Biodiesel Production. *Sci. World J.* **2013**, *2013*, 460923. https://doi.org/10.1155/2013/460923.
65. Fayyazi, E.; Ghobadian, B.; van de Bovenkamp, H.H.; et al. Optimization of Biodiesel Production over Chicken Eggshell-Derived CaO Catalyst in a Continuous Centrifugal Contactor Separator. *Ind. Eng. Chem. Res.* **2018**, *57*, 12742–12755. https://doi.org/10.1021/acs.iecr.8b02678.
66. Prameswari, J.; Widayat, W.; Buchori, L.; et al. Novel iron sand-derived α-$Fe_2O_3$/$CaO_2$ bifunctional catalyst for waste cooking oil-based biodiesel production. *Environ. Sci. Pollut. Res.* **2023**, *30*, 98832–98847. https://doi.org/10.1007/s11356-022-21942-z.
67. Echaroj, S.; Pannucharoenwong, N.; Duanguppama, K.; et al. High throughput biodiesel production from waste cooking oil over metal oxide binded with $Fe_2O_3$. *Energy Rep.* **2023**, *9*, 205–215. https://doi.org/10.1016/j.egyr.2023.05.271.
68. Shao, L.; Xu, J.; Saxén, H.; et al. A numerical study on process intensification of hydrogen reduction of iron oxide pellets in a shaft furnace. *Fuel* **2023**, *348*, 128375. https://doi.org/10.1016/j.fuel.2023.128375.
69. Sharifi, M.; Tangestaninejad, S.; Moghadam, M.; et al. Metal-organic frameworks-derived CaO/ZnO composites as stable catalysts for biodiesel production from soybean oil at room temperature. *Sci. Rep.* **2025**, *15*, 3610. https://doi.org/10.1038/s41598-025-87393-x.
70. Zhang, Y.; Niu, S.; Han, K.; et al. Synthesis of the SrO–CaO–$Al_2O_3$ trimetallic oxide catalyst for transesterification to produce biodiesel. *Renew. Energy* **2021**, *168*, 981–990. https://doi.org/10.1016/j.renene.2020.12.132.

71. Sivaprakash, G.; Mohanrasu, K.; Ravindran, B.; et al. Integrated approach: $Al_2O_3$-CaO nanocatalytic biodiesel production and antibacterial potential silver nanoparticle synthesis from *Pedalium murex* extract. *J. King Saud Univ. Sci.* **2020**, *32*, 1503–1509. https://doi.org/10.1016/j.jksus.2019.12.004.
72. Enguilo Gonzaga, V.; Romero, R.; Gómez-Espinosa, R.M.; et al. Biodiesel Production from Waste Cooking Oil Catalyzed by a Bifunctional Catalyst. *ACS Omega* **2021**, *6*, 24092–24105. https://doi.org/10.1021/acsomega.1c03586.